JOURNAL OF AIRCRAFT
Vol. 30, No. 6, Nov.–Dec. 1993

Computational Study of Blowing on Delta Wings at High Alpha

Ken Craig*
Stanford University, Stanford, California 94305

In this study, the flowfield produced by tangential leading-edge blowing on a rounded leading-edge 60-deg delta wing at high angle of attack is investigated computationally by solving the thin-layer Navier-Stokes equations. Steady-state flowfields are calculated for various angles of attack, with and without the presence of tangential leading-edge blowing. The numerical grid is generated using algebraic grid generation and various interpolation and blending techniques. The jet emanates from a slot with linearly varying thickness, and is introduced into the flowfield using the concept of an actuator plane, thereby not requiring resolution of the jet slot geometry. The Baldwin-Lomax algebraic turbulence model is used to provide turbulent closure. The computational results are compared with those of experiments. The effectiveness of blowing as a rolling moment control mechanism to extend the envelope of controllability is illustrated at different angles of attack. The saturation effect of increased blowing is captured well in the computations. Control reversal noted in similar experimental studies is also observed in the computations.

Nomenclature

AR	=	aspect ratio
b	=	wing maximum span
C_L	=	wing lift coefficient
C_{Mx}	=	wing rolling moment coefficient
C_N	=	wing normal force coefficient
Cp	=	pressure coefficient
Cp_{stag}	=	stagnation pressure coefficient
$C_\mu = \dot{m}_j U_j / q_\infty S_{ref}$	=	blowing momentum coefficient
M_∞	=	freestream Mach number
$\dot{m}_j$	=	jet mass flow rate
q_∞	=	dynamic pressure
Re	=	Reynolds number based on wing root chord
S_{ref}	=	wing reference area
t	=	wing thickness
U_j	=	jet velocity
x	=	streamwise coordinate
α	=	angle of attack
β	=	yaw angle

Introduction

THE extension of the high-angle-of-attack regime of delta wing aircraft has been of considerable interest in recent years. It is well known that the flow at high α over delta wings is dominated by two leading-edge vortices. Previous studies have shown the occurrence of vortex asymmetry and burst, the first of which can lead to the wing rock phenomenon. Both vortex asymmetry and burst cause nonlinear and often unpredictable aerodynamic forces and moments. Since conventional control surfaces are often ineffective at high α, it is desirable to have a mechanism that would control the strength and location of these leading-edge vortices, and therefore, control the aerodynamic forces.

By modifying the vortical flowfield, tangential leading-edge blowing (TLEB) has been shown experimentally[1] and computationally[2] to be a viable option in providing roll control for delta wings at high α. The studies in Refs. 1 and 2 were for a half-span wing assuming symmetry. More recently, experimental studies were performed using a full-span wing[3,4] where the effectiveness of TLEB was again demonstrated. Data from these studies include force and moment coefficients, as well as surface pressures and laser sheet flow visualization at one downstream station.

Previous computational studies[5–11] of the subsonic flow over delta wings at high α have mainly concentrated on wings with sharp leading edges where separation is generally fixed. A round leading edge necessitates the use of a viscous method in order to determine the exact location of the primary separation line. The accuracy of the location of the separation line plays an important role in both the prediction of the forces due to leading-edge suction, as well as the determination of the influence of the vortices.

This article describes a computational study solving the thin-layer form of the Navier-Stokes equations for the flow about the same full-span model as used in the aforementioned experiments.[3,4] The numerical grid is generated algebraically using various blending and interpolation functions. The jet slot is not modeled explicitly in the grid (as by Yeh et al.[2] for a half-span delta wing), but is introduced using the actuator plane concept as used by Tavella et al.[12] and Font and Tavella.[13] The flow is solved using the F3D code, which has been successfully applied to high α flow.[12–14] The Baldwin-Lomax half-equation algebraic turbulence model,[15] with modifications suggested by Degani and Schiff,[16] is used to provide turbulent closure.

The objectives of this study are 1) to validate the current approach by comparing computational results with that of experiment; 2) to provide a detailed description of the flowfield and aerodynamics governing the flow at angle of attack with and without the presence of blowing; and 3) to show the effectiveness of TLEB as a roll control mechanism at high angles of attack.

Geometry

The delta wing used for this numerical study has a leading-edge sweep angle of 60 deg and is shown in Fig. 1. The geometry is the same as that used for the experiments reported by Celik et al.[3] and Wood et al.[4] The leading edges are round, and the top and bottom surfaces of the wing are parallel with a constant thickness (6% at the root chord). The nose of the wing is generated by continuing the leading edges to the apex. The result of this is a sharp nose when viewed from above, but an elliptically shaped nose when viewed from the side. The wing is cropped to form a constant span tail or flap which

Presented as Paper 92-0410 at the AIAA 30th Aerospace Sciences Meeting, Reno, NV, Jan. 6–9, 1992; received April 20, 1992; revision received Aug. 6, 1992; accepted for publication Aug. 7, 1992.

*Doctoral Candidate, Department of Aeronautics and Astronautics; currently Lecturer, Department of Mechanical and Aeronautical Engineering, University of Pretoria, South Africa. Student Member AIAA.

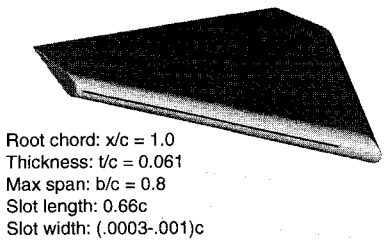

Fig. 1 Perspective view of wing with blowing slot.

is angled on the lower surface. The jet slot for blowing is situated on the pilot's right wing leading edge from the nose-body junction, to just short of the beginning of the wing tail.

Grid Generation

Due to the relatively simple grid topology required for this geometry, the grid about the delta wing is generated algebraically. Algebraic grid generation is efficient and therefore lends itself to grid refinement studies. The grid is generated in two-dimensional sections and stacked together. Several postprocessing steps are then performed, mainly through interpolation, to redistribute points in three-dimensional space to account for expected regions of high gradients. The two-sided stretching function of Vinokur[17] is employed in the redistribution.

Topology

The grid topology is C-O. There are three sections in the original grid. The first is the nose that has a spherical cap. The generation of this cap is done in two-dimensional semicircular disks that are stacked in the circumferential direction. The second section is the body of the wing where two-dimensional downstream cross sections or crossflow planes are generated. In cross section, the leading edge is elliptical since it is circular normal to the leading edge. The last section is the tail-wake region where two-dimensional downstream sections are again generated. Cross sections of the tail are rectangular due to the cropped wing. A zero-thickness wake with flow-through boundary conditions is added to the wing to allow for closure of the computational domain.

Stretching is employed in the downstream direction on the wing body and in the wake. Since the flow conditions to be studied are subsonic, the grid extends six chord lengths upstream and nine chord lengths downstream of the wing.

Orthogonality

As suggested by Tavella,[18] an algebraic grid can be improved by postprocessing, particularly by blending onto desired functions close to a body surface. This is implemented by projecting the arc lengths of the existing grid at a surface onto normals to the surface, and then blending the existing grid and the normals by using an inverse tangent function combination. The blending function is given by the following equation:

$$x(l) = x_1(l)f_1 + x_2(l)f_2$$

where

$$f_1 = (2/\pi)\tan^{-1}[(l/L_t)^p]$$
$$f_2 = (2/\pi)\tan^{-1}[(L_t/l)^p]$$

L_t = transition index
p = power
x = generic coordinate
l = index

The number of intervals blended, the grid location where the two functions being blended coincide (transition index), and the power of the blending function need to be specified. Trial values for these three parameters are NL, $0.4NL$, and 4, respectively, where NL is the total number of grid points

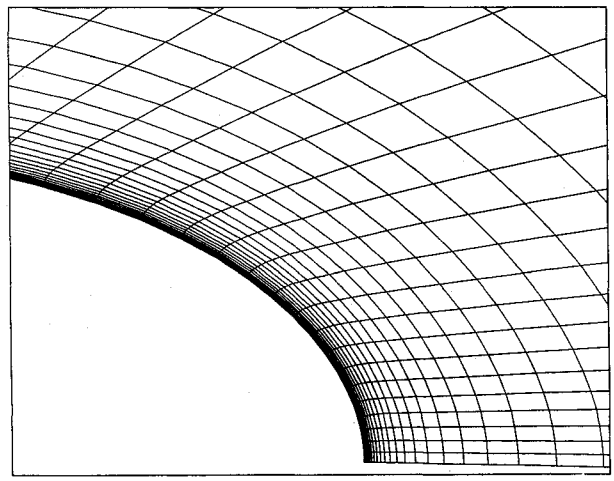

Fig. 2 Close-up of nose grid showing effect of blending.

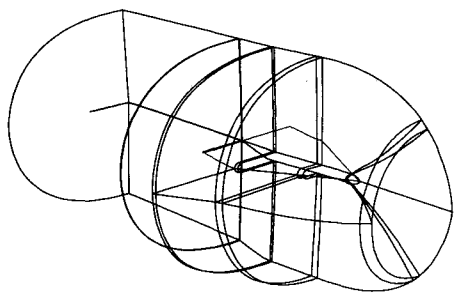

Fig. 3 Zonal arrangement.

in the normal direction. The surface normal is determined by defining two body-tangent vectors at each surface grid point. The cross product of these two vectors divided by its length gives the unit normal $\boldsymbol{n}$. From the unit normal, we can calculate a projection matrix $\boldsymbol{P} = \boldsymbol{n}^T\boldsymbol{n}/\boldsymbol{n}\cdot\boldsymbol{n}$ which when post-multiplied by any vector, would give the projection of that vector along the unit normal. A cross section of the grid shown in Fig. 2 illustrates the result of blending.

Zonal Arrangement

The implementation of the flow solver requires multiple zones of a certain maximum size each because of memory limitations. To accommodate this, the grid is divided into 14 zones. No interpolation is required at the zonal interfaces. Symmetric zones are used to save on secondary storage because the metrics are identical for both sides of the symmetry plane.[12] The zones are separated circumferentially at the blowing slots for the implementation of the actuator plane as an interzonal boundary condition. The total grid is 80 × 137 × 50 in the streamwise, spanwise, and normal directions, or 548,000 points. The total Cray Y-MP CPU time required is 23 s for the generation of a grid of this size. The zonal arrangement is shown in Fig. 3.

Numerical Method

The flow is solved for using a version of the F3D code that contains the algorithm developed by Steger et al.[19,20] The implicit two-factor algorithm uses flux-vector splitting to upwind difference the convection terms in the streamwise direction, while retaining central differencing in the other directions. This scheme is unconditionally stable for the model wave equation and can have natural numerical dissipation and better stability properties than fully central difference algorithms.[19]

Due to the high Reynolds number flow in this study, the Baldwin-Lomax turbulence model,[15] with modifications for

crossflow separation suggested by Degani and Schiff,[16] is used. Values for y^+ are consistently less than four throughout the grid. The wake is assumed to be laminar. The flow on the wing is treated as fully turbulent.

Freestream boundary conditions are used for the far-field boundaries, while the body surface is treated as no-slip. A typical CPU time is 30 s/iteration/time step on a Cray Y-MP. Steady-state flow solutions are obtained in 3000–10,000 steps, depending on the initial conditions.

Actuator Plane Concept

The difference between using the actual geometry and using the actuator plane concept is illustrated in Fig. 4. Note that the actuator plane is, in effect, a discontinuity imposed as a boundary condition in the flow at an interzonal boundary. This concept has been used before on an ogive cylinder[13] and the F-18 forebody.[12] In the latter study, a comparison was made between resolving and not resolving the jet slot. The differences in results were found to be minimal for a delta wing test case.

The jet Mach number is calculated assuming incompressibility and with the jet exit pressure equal to that of freestream. The boundary condition at the jet interface of the zone below the jet is obtained by extrapolation from the interior points.

Results and Discussion

All cases were run at $M_\infty = 0.2$ and $Re = 1.2 \times 10^6$ based on the wing root chord.

No Blowing Cases

$\alpha = 30$ deg, $\beta = 0$ deg

Figures 5 and 6 show the computed surface flow patterns and particle traces, respectively, for this case. Note that at this α, the vortex remains unburst until it reaches the tail portion of the wing. Bursting is evident from the sudden thickening of the core in the particle traces. In Fig. 5, the primary separation line extends along the leading edge and moves outboard. This variation in separation location is one of the main differences between this wing and a sharp leading-edge wing where the primary separation line is usually fixed at the leading edge itself.

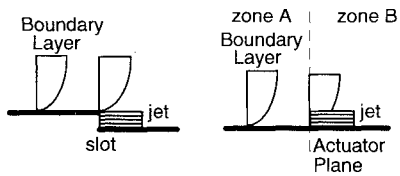

Fig. 4 Actuator plane concept.

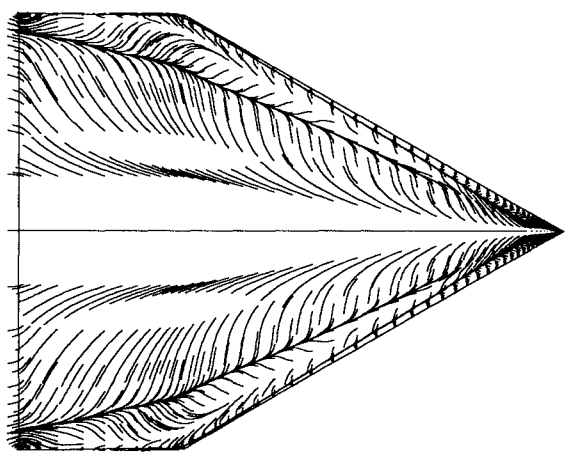

Fig. 5 Computed surface flow patterns ($\alpha = 30$ deg, $\beta = 0$ deg).

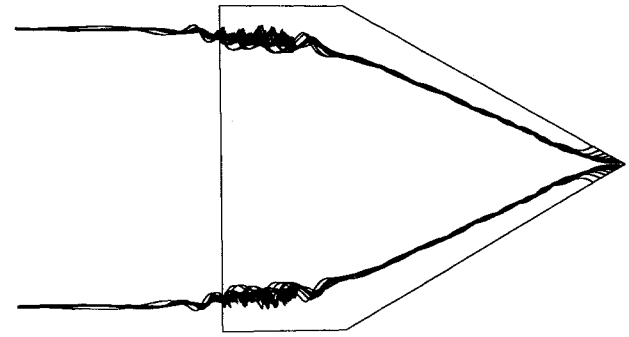

Fig. 6 Particle traces ($\alpha = 30$ deg, $\beta = 0$ deg).

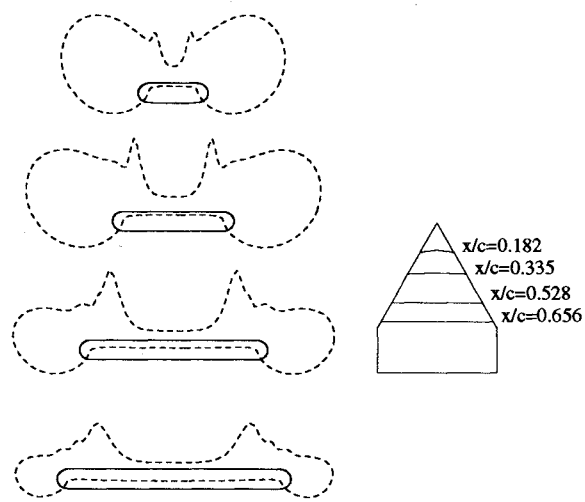

Fig. 7 Normal pressure coefficient distributions ($\alpha = 30$ deg, $\beta = 0$ deg).

Figure 7 gives the calculated spanwise pressure coefficient distributions at four downstream stations. To illustrate the large influence of the rounded leading edge of the wing, the pressure coefficient is plotted normal to the surface of the wing cross section. The outward normal represents suction, while a positive pressure coefficient would be "into" the wing as is shown on the lower surface. This representation is often used for roughly circular cross-sectional bodies and will be shown to be informative here. Note that the formation of the primary vortex is again evident. The evidence of secondary vortices can be seen in the secondary pressure peaks at the $x/c = 0.528$ and 0.656 locations. A signature of a rounded leading-edge wing is clearly visible in the form of a wide leading-edge suction peak, or lobe, especially in the upstream locations. For sharp leading-edge wings, this peak is often only a spike, thereby, not contributing significantly to the lift.

$\alpha = 50$ deg, $\beta = 0$ deg

Figures 8 and 9 show the computed surface flow and particle traces for this case. At this α, vortex breakdown is observed at 30% root chord approximately. The breakdown can be described as both bubble and spiral type because of both elements being visible in the particle traces. The surface flow patterns on the tail show a saddle point under the stagnated flow of the burst vortex. From a study of side views of the particle traces, the vortex trajectory remains close to the wing due to the suction on the vortex and then follows the freestream direction in the wake.

Figure 10 gives the calculated pressure coefficient distributions at the same four downstream stations for this case. The footprint of a burst vortex in this case is a flattening of the vortex suction pressure peak and a reduction of the leading-edge suction lobe in the downstream locations.

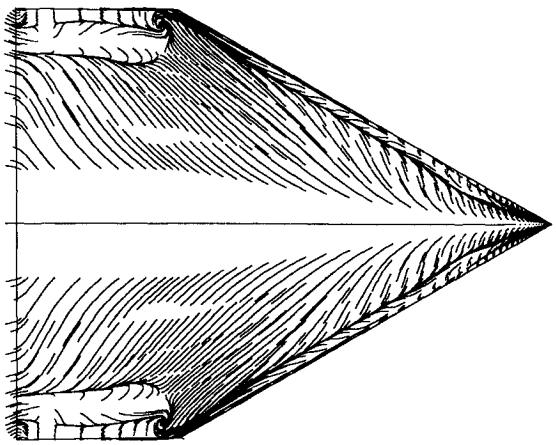

Fig. 8 Computed surface flow patterns (α = 50 deg, β = 0 deg).

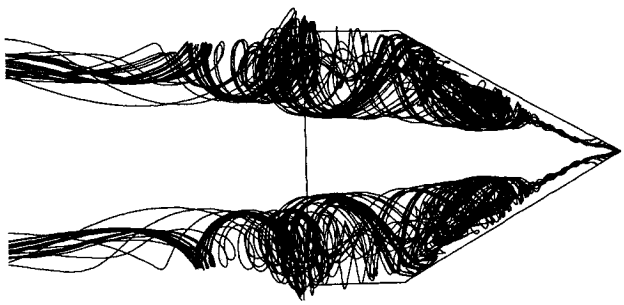

Fig. 9 Particle traces (α = 50 deg, β = 0 deg).

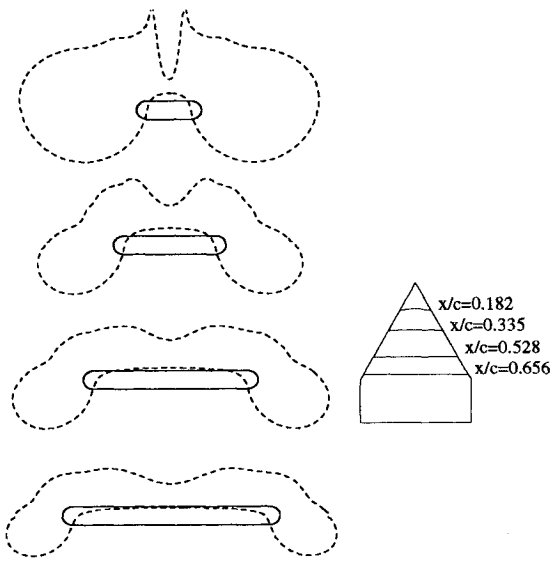

Fig. 10 Normal pressure coefficient distributions (α = 50 deg, β = 0 deg).

Comparison with Experiment

Before comparisons are made, it should be noted that the experiments[3,4] were run at $M_\infty = 0.058$, $Re = 4 \times 10^5$, and $M_\infty = 0.12$, $Re = 8 \times 10^5$ for all α and β cases, and that significant wind-tunnel wall interference at high α was noted[4] due to a relatively small test section. In addition, the model support section and tubing required for blowing in the experiment are also expected to influence the comparison. It should be pointed out, however, that the aim of the experiment was to show the effect of blowing, and therefore, the difference in coefficient values between the blown and unblown cases, rather than the absolute values of the coefficients. Reservations have also been expressed[4] as to the accuracy of the stall angle and burst locations, in view of comparisons with other similar experiments. Therefore, comparison studies between computation and experiment should only be made if the differences between blown and unblown coefficients are used. The subsonic computations are run at a higher Mach number than experiment, namely 0.2, since this is the lowest practical Mach number for which converged solutions of the Navier-Stokes equations can be reasonably obtained.

First, a comparison of the lift coefficient is made. Figure 11 shows the computational C_L values for the α = 30-deg, β = 0-deg and α = 50-deg, β = 0-deg cases as compared to the leading-edge suction analogy theory of Polhamus[21] for incompressible flow and experiments[11,22-24] on sharp leading-edge wings at comparable AR. The tail on the wing under study gives it an effective AR = 1.224. The Polhamus analogy is for sharp leading edge and pure delta wings, and is therefore only useful in qualitative comparisons. The theory is only expected to be accurate for α before breakdown occurs.[21] The poor agreement between the sharp leading-edge experiments and the present rounded leading-edge computations at α = 50 deg is due to the fact that the stall angle of attack is very different due to the difference in roundness and thickness, and that the wings have different sweep angles (60 deg for the computations and 70 deg for most of the experiments). Unfortunately, only normal force coefficients (no lift or drag coefficients) were measured in the experiments,[3,4] so a direct comparison of lift is not possible. An indirect comparison is made by including the component of the normal force in the lift direction, i.e., $C_N \cos \alpha$, in Fig. 10. This value approaches C_L as α is increased.

Recent experimental results were reported with a similar wing at the University of Bath.[25] In the Stanford experiments,[4] the value of C_N at α = 30 deg was about 1.8, whereas for the Bath experiments, it was about 1.4, another indication of the influence of wind-tunnel walls. In the computations the value is about 1.2.

Soltani et al.[22] showed that an increase in Reynolds number decreases the vortex lift at a given α. This could partly explain why the normal force coefficient values of the computations are below that of experiment.

Grid Refinement

A limited grid refinement study was made to investigate the grid dependency of the solution. A solution of the α = 30-deg case was obtained for a grid of 80 × 137 × 80, or 876,800 points. The solution stayed virtually unchanged in the vortex region, although some limited change was noted in the leading-edge region. This led to some confidence that the size grid used in this study, while not fine enough to provide totally grid independent solutions, is fine enough to satisfy the current objectives. Reference 26 provides more detail on the refinement.

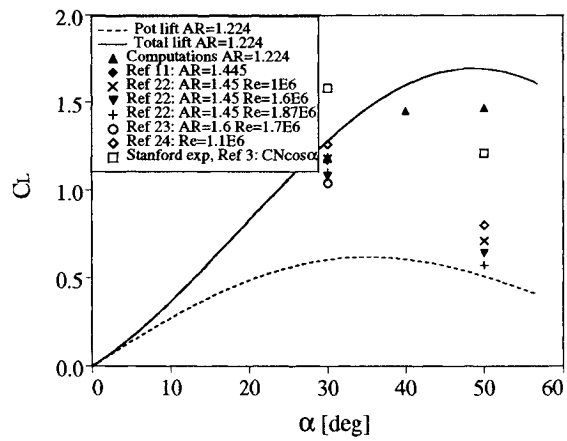

Fig. 11 Comparison of (α = 30 deg, β = 0 deg) and (α = 50 deg, β = 0 deg) lift coefficient with Polhamus theory[21] and experiment.

Blowing Cases

Comparison of Rolling Moment Coefficient with Experiment

Figure 12 gives the rolling moment comparison for the α = 30-deg case as compared to experiment.[3] A negative rolling moment corresponds to a blown-side-up rolling moment. Note how the saturation effect is captured well by the computations. This confirms the conclusion in the experimental study[4] that blowing for a prestall angle of attack is only useful in a limited range. Since the rolling moment is zero at zero blowing, the figure actually shows the difference in rolling moment coefficient between blowing and no blowing.

α = 30 deg, β = 0 deg

A range of blowing coefficients was used to effectively show the influence of blowing on the aerodynamics. From the experiments,[3,4] a value of C_μ of about 0.04 marks the boundary of the useful blowing region. Increasing the blowing intensity further produced no increase in rolling moment at this prestall angle of attack. To capture this nonlinear behavior in the computations, a range of C_μ from 0 to 0.06 was chosen in increments of 0.01.

The effect of tangential leading-edge blowing on the flow at this α for three blowing coefficients is shown in the particle traces of Fig. 13. The blowing slot is on the pilot's right. Note how an increase in blowing intensity effectively moves the leading-edge vortex inboard until, at some blowing coefficient, the flow becomes completely attached. The unblown side vortex then becomes entrained into, or wraps around, the unblown side primary vortex. At this α, the flow on the unblown side remains essentially unchanged by the blowing, and is therefore, uncoupled. At lower C_μ values, the leading-edge vortex on the blown side is not as focused or as strong as the one on the unblown side.

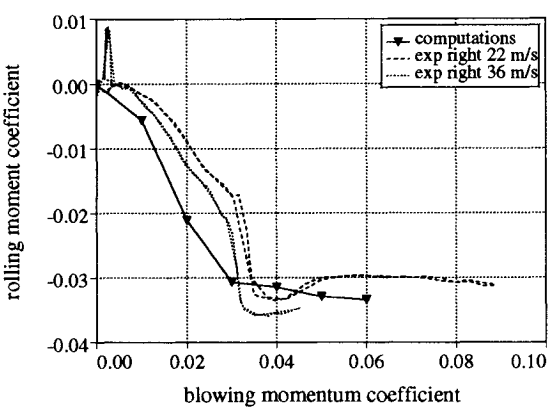

Fig. 12 Comparison of rolling moment coefficient as a function of blowing momentum coefficient between computations and experiment[3] (α = 30 deg, β = 0 deg).

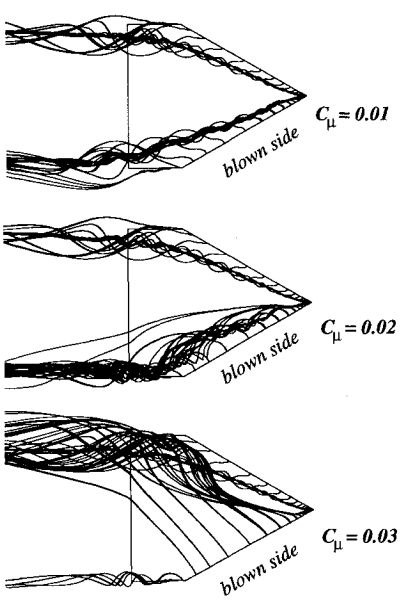

Fig. 13 Particle traces (α = 30 deg, β = 0 deg, C_μ = 0.01, 0.02, 0.03).

Figure 14 shows the computed surface flow patterns. Here, the effectiveness of blowing in moving the primary separation line is evident. Note that at the highest blowing coefficient shown, the surface flow goes over the symmetry line up to the unblown side secondary separation line, where it leaves the surface.

The calculated spanwise pressure coefficients at the 33.5% downstream station for increasing values of blowing intensity are shown in Fig. 15, looking forward. The uncoupling is evident in the constancy of the unblown side curves. On the blown side, the weakening of the primary leading-edge vortex with increased blowing (C_μ = 0.01–0.03) can be seen. The lift and rolling moment contributions of the leading-edge suction peak increase with increased blowing until higher values of C_μ, where the Coanda-effect pressure signature of the leading-edge suction stays constant.

α = 50 deg, β = 0 deg

Flow solutions for three values of C_μ were calculated for this case. The pressure distributions for two cases are given in Fig. 16, again shown looking forward. In the forward location, blowing weakens the blown side vortex, and the leading-edge suction is less on the lower surface than on the upper. From the breakdown location aft, blowing increases the strength and unbursts the blown side vortex. Control reversal is observed for the low value of C_μ. The unblown side vortex is unburst so that its pressure suction peak is higher than the blown side. In addition, the leading-edge suction lobe caused by the Coanda-effect of the jet is still smaller than the lower surface leading-edge suction. Both contribute to a blown-side down-rolling moment. As blowing is increased, the Coanda suction lobe grows, and the unblown side vortex strength decreases, combining to roll the wing the other way, i.e., blown-side wing up.

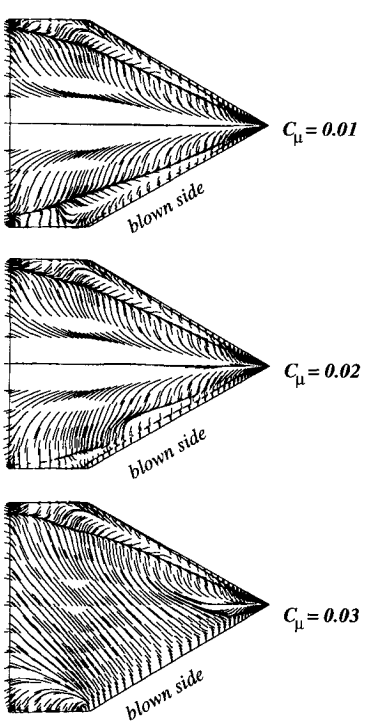

Fig. 14 Computed surface flow patterns (α = 30 deg, β = 0 deg, C_μ = 0.01, 0.02, 0.03).

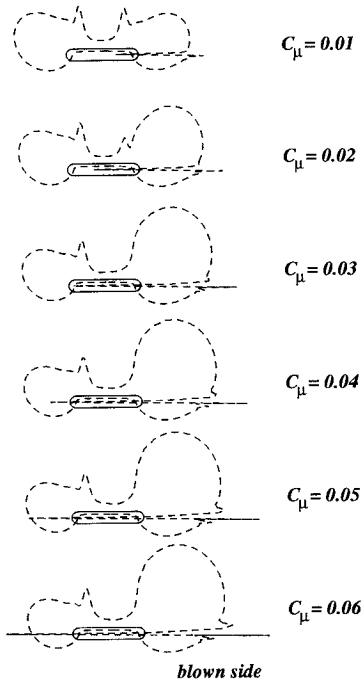

Fig. 15 Normal pressure coefficient as function of blowing at 33.5% downstream station (α = 30 deg, β = 0 deg).

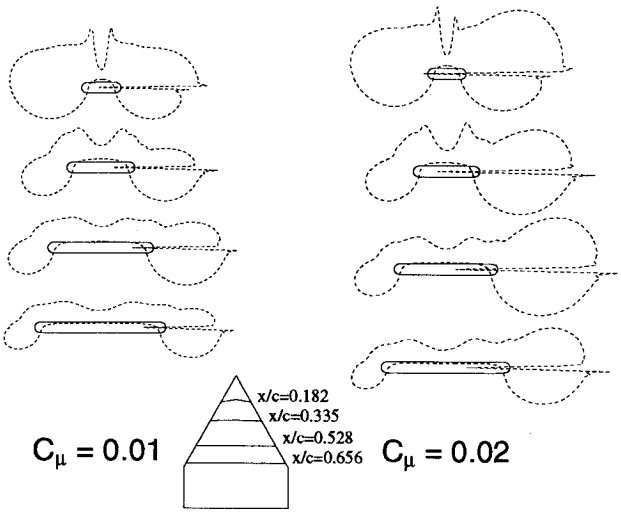

Fig. 16 Normal pressure coefficient distributions (α = 50 deg, β = 0 deg, C_μ = 0.01, 0.02, 0.04).

Control Reversal

As noted above, control reversal was obtained only at the condition α = 50, β = 0 deg, C_μ = 0.01. Figure 17 shows a comparison of the rolling moment coefficient contours in α-C_μ space for the Stanford and Bath experiments taken from Ref. 25. The planforms of the wings have the same sweep, but the aspect ratios are 1.224 and 1.582, and the thicknesses are 6 and 3.3%, respectively. The blowing slots are different, but more importantly, wind-tunnel wall interference is much less for the Bath experiments where the wing/tunnel area ratio was only 5% at α = 90 deg. The contours show the same basic control reversal, but for the Bath case it is confined to the stall angles of attack. For instance, at α = 50 deg, control reversal occurred in the Stanford experiments, but not in the Bath experiments. The reversal would appear to occur at a similar angle relative to the wing stall. Hence, the wall interference modifies the stall angle, and thus, the reversal angle. From the limited number of cases run computationally, it would seem that the pocket of control reversal in α-C_μ space

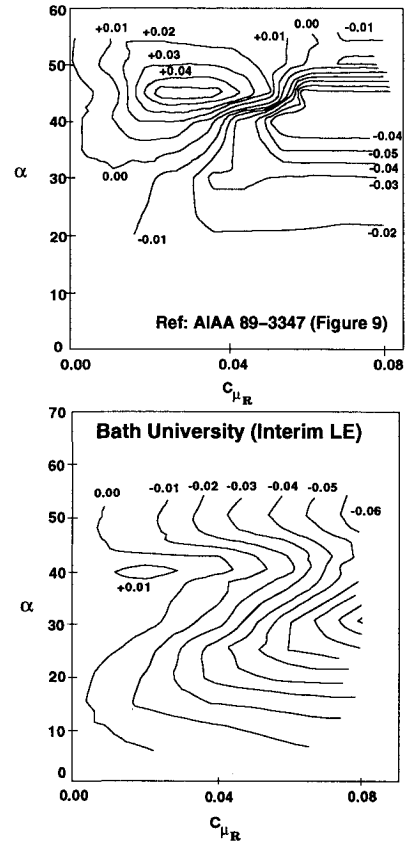

Fig. 17 Comparison of rolling moment coefficient countours in α-C_μ space between Stanford[3,4] and Bath[25] experiments.

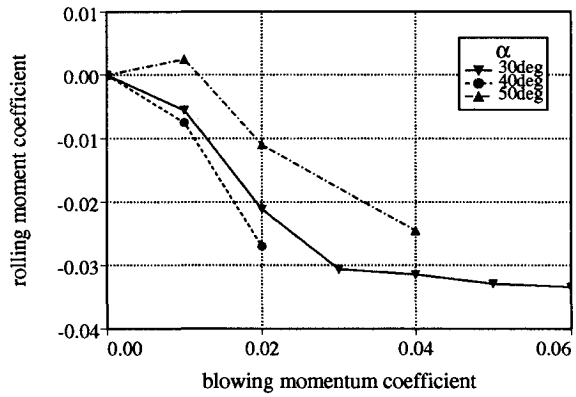

Fig. 18 Computed rolling moment coefficient as a function of blowing momentum coefficient (α = 30, 40, and 50 deg).

is at a slightly higher α than in the Bath case. All the calculated values of rolling moment vs blowing momentum coefficient are shown in Fig. 18, confirming the control reversal in the one α = 50-deg case.

Conclusions

This study shows that a successful calculation of the complicated flowfield around a rounded leading-edge delta wing at angles of attack, with and without tangential leading-edge blowing, is possible with current resources. The results obtained thus far compare reasonably well with experiments if the difference in coefficients between unblown and blown cases is used. The effectiveness of blowing as a way to provide roll control at high angles of attack is illustrated. The saturation effect of increased blowing was captured well. Control reversal noted in experiments is also observed in the computations.

Acknowledgments

The author wishes to thank the Fixed Wing Aerodynamics Branch at NASA Ames Research Center for their support and the use of their facilities. The author also wishes to thank Leonard Roberts, Eugene Tu, and Domingo Tavella for their support.

References

[1]Wood, N. J., and Roberts, L., "Control of Vortical Lift on Delta Wings by Tangential Leading-Edge Blowing," *Journal of Aircraft*, Vol. 25, No. 3, 1988, pp. 236–243.

[2]Yeh, D., Tavella, D., Roberts, L., and Fujii, K., "Numerical Study of the Effect of Tangential Leading-Edge Blowing on Delta Wing Vortical Flow," AIAA Paper 89-0341, Jan. 1989.

[3]Celik, Z. Z., Roberts, L., and Wood, N. J., "An Investigation of Asymmetric Vortical Flows over Delta Wings with Tangential Leading-Edge Blowing at High Angles of Attack," AIAA Paper 90-0103, Jan. 1990.

[4]Wood, N. J., Roberts, L., and Zelik, Z., "Control of Asymmetric Vortical Flows over Delta Wings at High Angles of Attack," *Journal of Aircraft*, Vol. 27, No. 5, 1990, pp. 429–435.

[5]Smith, J. H. B., "Improved Calculation of Leading Edge Separation from Slender Thin Delta Wings," *Proceedings of the Royal Society, Series A*, Vol. 306, 1968, pp. 67–99.

[6]Kandil, O. A., and Chuang, H. A., "Unsteady Navier-Stokes Computations Past Oscillating Delta Wing at High Incidence," AIAA Paper 89-0081, Jan. 1989.

[7]DeJarnette, F. R., and Shawn, H. W., "Numerical Determination of Secondary Separation on Delta Wings in Subsonic Flow," *Journal of Aircraft*, Vol. 22, No. 7, 1985, pp. 602–608.

[8]Hsu, C.-H., and Hartwich, P.-M., "Computation of Vortical Interaction for a Sharp-Edged Double-Delta Wing," *Journal of Aircraft*, Vol. 25, No. 5, 1988, pp. 442–447.

[9]Krist, S. L., Thomas, J. L., Sellers, W. L., and Kjelgaard, S. O., "An Embedded Grid Formulation Applied to a Delta Wing," AIAA Paper 90-0429, Jan. 1990.

[10]Gordnier, R. E., and Visbal, M. R., "Unsteady Navier-Stokes Solutions for a Low Aspect Ratio Delta Wing," AIAA Paper 90-1538, June 1990.

[11]Deese, J. E., Agarwal, R. K., and Johnson, J. G., "Calculation of Vortex Flowfields Around Forebodies and Delta Wings," AIAA Paper 90-0176, Jan. 1991.

[12]Tavella, D. A., Schiff, L. B., and Cummings, R. M., "Pneumatic Vortical Flow Control at High Angles of Attack," AIAA Paper 90-0098, Jan. 1990.

[13]Font, G., and Tavella, D., "High Alpha Aerodynamic Control by Tangential Fuselage Blowing," AIAA Paper 91-0620, Jan. 1991.

[14]Ekaterinaris, J. A., and Schiff, L. B., "Vortical Flows over Delta Wings and Numerical Prediction of Vortex Breakdown," AIAA Paper 90-0102, Jan. 1990.

[15]Baldwin, B. S., and Lomax, H., "Thin Layer Approximation and Algebraic Model for Separated Turbulent Flows," AIAA Paper 78-0257, Jan. 1978.

[16]Degani, D., and Schiff, L. B., "Computation of Turbulent Supersonic Flows Around Pointed Bodies Having Crossflow Separation," *Journal of Computational Physics*, Vol. 66, 1986, pp. 173–196.

[17]Vinokur, M., "On One-Dimensional Stretching Functions for Finite-Difference Calculations," *Journal of Computational Physics*, Vol. 50, 1983, pp. 215–234.

[18]Tavella, D. A., private communication, Stanford Univ., Stanford, CA, June 1990.

[19]Steger, J. L., Ying, S. X., and Schiff, L. B., "A Partially Flux-Split Algorithm for Numerical Simulation of Unsteady Viscous Flows," *Proceedings of Workshop on CFD*, Univ. of California, Davis, CA, 1986.

[20]Ying, S. X., Steger, J. L., Schiff, L. B., and Baganoff, D., "Numerical Simulation of Unsteady, Viscous High Angle of Attack Flows Using a Partially Flux-Split Algorithm," AIAA Paper 86-2179, 1986.

[21]Polhamus, E. C., "Prediction of Vortex-Lift Characteristics by a Leading-Edge Suction Analogy," *Journal of Aircraft*, Vol. 8, No. 4, 1971, pp. 193–199.

[22]Soltani, M. R., Bragg, M. B., and Brandon, J. M., "Measurements on an Oscillating 70-Deg Delta Wing in Subsonic Flow," *Journal of Aircraft*, Vol. 27, No. 3, 1990, pp. 211–217.

[23]Wentz, W. H., "Wind Tunnel Investigations of Vortex Breakdown on Slender Sharp-Edged Wings," Ph.D. Dissertation, Univ. of Kansas, Lawrence, KS, 1968.

[24]Hummel, D., and Srinivasan, P. S., "Vortex Breakdown Effects on the Low-Speed Characteristics of Slender Delta Wings in Symmetrical Flow," *Journal of the Royal Aeronautical Society*, Vol. 71, April 1967, pp. 319–322.

[25]Greenwell, D. I., and Wood, N. J., "Control of Asymmetric Vortical Flows," AIAA Paper 91-3272-CP, Sept. 1991.

[26]Craig, K. J., "Computational Study of the Aerodynamics and Control by Blowing of Asymmetric Vortical Flows over Delta Wings," Ph.D. Dissertation, Stanford Univ., Stanford, CA, Aug. 1992.